Available online at www.sciencedirect.com
SCIENCE DIRECT®
PERGAMON
International Journal of Heat and Mass Transfer 46 (2003) 3041–3050
International Journal of HEAT and MASS TRANSFER
www.elsevier.com/locate/ijhmt

Effect of compressibility on gaseous flows in micro-channels

Yutaka Asako [a,*], Tianqi Pi [a], Stephen E. Turner [b], Mohammad Faghri [b]

[a] Department of Mechanical Engineering, Tokyo Metropolitan University, 1-1 Minami-Osawa, Hachioji, Tokyo 192-0397, Japan

[b] Department of Mechanical Engineering and Applied mechanics, University of Rhode Island, Kingston, RI 01882-0805, USA

Received 7 August 2002; received in revised form 16 December 2002

Abstract

Two-dimensional compressible momentum and energy equations are solved in a parallel plate channel to obtain the effect of compressibility on gaseous flow characteristics in micro-channels. The numerical methodology is based on arbitrary-Lagrangian–Eulerian method. The computations were performed for a wide range of Reynolds number and Mach number and for both 'no heat conduction' and isothermal flow conditions. The results are presented in form of the product of friction factor and Reynolds number ($f \cdot Re$) expressed as a function of both Reynolds number and Mach number and was compared with available experimental results. It was found that $f \cdot Re$ is mainly a function of Mach number and is different from the incompressible value of 96 for parallel-plate channels.

1. Introduction

Fabrication of small devices has increased the needs for understanding of fluid flow and heat transfer in micro-geometries. Since the early work of Tuckerman and Pease [1], many experimental and numerical investigations have been undertaken. Wu and Little [2] performed experimental studies of gaseous flows in micro-channels to obtain friction factor and Nusselt number for nitrogen, argon and helium flows. The channels were etched in silicon and glass ranging in depth from 28 to 65 μm. The relative roughness was estimated to be as high as 0.2–0.3. Measured friction factors were higher than those predicted by the Moody's chart. Pfahler et al. [3] performed several experimental studies of liquid and gaseous flows in shallow micron and submicron channels to investigate the flow and heat transfer characteristics of flows in micro-channels. The channels depth was 0.5–38.7 μm and the typical surface roughness was of order of 1% as measured by a surface profilometer. Choi et al. [4] performed experiments to obtain friction factor and convective heat transfer coefficients for laminar and turbulent gas flow in micro-tubes having the relative roughness in the range of 0.0002–0.0116. The measured friction factors were below those predicted by Moddy's chart.

As can be seen, there are inconsistencies in the experimental data reported by different researchers. For examples, the product of the friction factor and Reynolds number, ($f \cdot Re$), was higher or lower than the conventional value ($f \cdot Re = 96$ for a conventional parallel-plate duct). Measured values of $f \cdot Re$ by Pfahler et al. [3] and Choi et al. [4] are lower than the conventional values but the results by Wu and Little [2] are higher. Furthermore, the measured values of $f \cdot Re$ by Pfahler et al. [3] and Choi et al. [4] increased as Re increased rather than being a constant. Several factors are attributed to this inconsistency. The rarefaction (the slip on the surface), the surface roughness and the compressibility might have significant effect on these results. These effects separately or combined might affect the experimental results.

The rarefaction effect can be studied by solving the momentum and energy equations with slip velocity and temperature jump boundary conditions (e.g., [5,6]). This effect is dominant when the characteristic length of the channel is less than about 10 μm. The value of $f \cdot Re$ decreases from the conventional value with decreasing characteristic length. Experimental studies of gaseous flows in micron channels with rough surface [2] and

* Corresponding author. Tel.: +81-426-77-2711; fax: +81-426-77-2701.
E-mail address: asako@ecomp.metro-u.ac.jp (Y. Asako).

0017-9310/03/$ - see front matter © 2003 Elsevier Science Ltd. All rights reserved.
doi:10.1016/S0017-9310(03)00074-7

Nomenclature

f_d	Darcy's friction factor, Eq. (19)
f_f	Fanning's friction factor, Eq. (20)
h	channel height (m)
i	specific internal energy (J/kg)
I	dimensionless internal energy, Eq. (11)
ℓ	channel length (m)
Ma	Mach number, Eq. (11)
p	pressure (Pa)
P	dimensionless pressure, Eq. (11)
q	heat generation per unit volume (J/m^3)
R	gas constant (J/(kg K))
Re	Reynolds number, Eq. (11)
T	temperature (K)
t	time (s)
u, v	velocity components (m/s)
U, V	dimensionless velocity components, Eq. (11)
x, y	coordinates (m)
X, Y	dimensionless coordinates, Eq. (11)
ϕ	dissipation function, Eq. (5)
Φ	non-dimensional dissipation function, Eq. (17)
γ	specific heat ratio (–)
μ	viscosity (Pa s)
ρ	density (kg/m^3)
ρ^*	dimensionless density, Eq. (11)

Subscripts

in	inlet
out	outlet
ref	reference cross-section
stg	stagnation value

smooth surface [3] have been performed and reported in the literature.

Compressibility effect have been reported by Prud'homme et al. [7] who performed a two-dimensional analysis of isothermal, laminar flow of an ideal gas in a straight micro-tube. Also, Berg et al. [8] performed a two-dimensional analysis of isothermal, laminar flow of ideal gas in a straight micro-tube. The range of the solutions is limited to low Ma number flows. The value of $f \cdot Re$ is higher but almost equal to the conventional value. Sayegh et al. [9] obtained the value of $f \cdot Re$ for a rarefied flow for $Kn = 0.009$ by direct simulation Monte Carlo (DSMC). This work was extended by Sun and Faghri [10] to study the effect of compressibility and rarefaction on gaseous flow in a micro-channel using DSMC. Also, Guo and Wu [11] performed computational investigations on compressibility effect in micro-tubes and found its effect to be important. Recently, Araki et al. [12,13] obtained the average friction factor for gaseous flow through micro-tubes and micro-channels experimentally and noted the effect of the compressibility. The effects of surface roughness, rarefaction and compressibility was experimentally investigated by Turner et al. [14,15]. This was the first study to systematically investigate the problem by isolating the effects of compressibility from rarefaction and surface roughness. The local pressure along the channel was measured, but only the average friction factor between the first and the last pressure taps was reported.

As can be seen above, there seems to be no literature on the parametric study of compressibility effect on local friction factor. The motivation of this work is to conduct numerical computations to obtain local friction factor for gaseous flow in parallel-plate ducts, for a wide range of Reynolds number and Mach number and compare the results with available experiments.

2. Formulation

2.1. Description of the problem and conservation equations

The problem is modeled as a parallel-plated channel as shown in Fig. 1 with a chamber at the stagnation temperature, T_{stg}, and the stagnation pressure, p_{stg}, attached to its upstream section. The flow is assumed to be steady, two-dimensional and laminar. The fluid is assumed to be an ideal gas with a specific heat ratio of $\gamma = 1.4$ and a gas constant of $R = 287$ J/(kg K). First, attention will be turned to the thermal conductivity of the gas. If the gas has zero thermal conductivity, the largest change in temperature will be observed along the channel. On the other hand, if the gas has an infinite thermal conductivity, the gas temperature will remain uniform. The former assumption may be referred to as 'no heat conduction' flow condition and the latter case may be called isothermal flow condition. The numerical

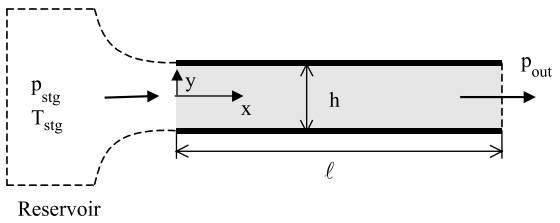

Fig. 1. A schematic diagram of problem.

analyses will be performed for both cases. The governing equations can be expressed as

$$\frac{\partial \rho u}{\partial x}+\frac{\partial \rho v}{\partial y}=0 \tag{1}$$

$$\frac{\partial \rho uu}{\partial x}+\frac{\partial \rho uv}{\partial y}=-\frac{\partial p}{\partial x}+\mu\left(\frac{\partial^2 u}{\partial x^2}+\frac{\partial^2 u}{\partial y^2}\right)+\frac{\mu}{3}\frac{\partial}{\partial x}\left(\frac{\partial u}{\partial x}+\frac{\partial v}{\partial y}\right) \tag{2}$$

$$\frac{\partial \rho uv}{\partial x}+\frac{\partial \rho vv}{\partial y}=-\frac{\partial p}{\partial y}+\mu\left(\frac{\partial^2 v}{\partial x^2}+\frac{\partial^2 v}{\partial y^2}\right)+\frac{\mu}{3}\frac{\partial}{\partial y}\left(\frac{\partial u}{\partial x}+\frac{\partial v}{\partial y}\right) \tag{3}$$

The energy equation for the 'no heat conduction' flow condition can be expressed as

$$\frac{\partial \rho ui}{\partial x}+\frac{\partial \rho vi}{\partial y}=-p\left(\frac{\partial u}{\partial x}+\frac{\partial v}{\partial y}\right)+\phi \tag{4}$$

where

$$\phi=2\mu\left[\left(\frac{\partial u}{\partial x}\right)^2+\left(\frac{\partial v}{\partial y}\right)^2\right]-\frac{2\mu}{3}\left(\frac{\partial u}{\partial x}+\frac{\partial v}{\partial y}\right)^2+\mu\left(\frac{\partial u}{\partial y}+\frac{\partial v}{\partial x}\right)^2 \tag{5}$$

As can be seen, heat conduction terms are neglected for the case of the 'no heat conduction flow' condition. The energy equation for the isothermal flow condition can be expressed as

$$i=i_{\mathrm{in}} \tag{6}$$

where i_{in} is the specific internal energy at the inlet. Namely, the channel wall temperature is the same as the fluid temperature at the inlet. The equation of the state for the ideal gas can be expressed by

$$i=\frac{1}{\gamma-1}\frac{p}{\rho} \tag{7}$$

Furthermore, with the assumptions of no slip boundary condition, uniform inlet velocity, pressure and density and specified pressure, p_{out}, at the outlet, the boundary conditions can be expressed as follows:

$$\begin{aligned}&\text{on the walls } (y=\pm 0.5h):\ u=v=0\\&\text{at the inlet } (x=0):\ u=u_{\mathrm{in}},\ v=0,\ p=p_{\mathrm{in}},\ \rho=\rho_{\mathrm{in}}\\&\text{at the outlet } (x=\ell):\ p=p_{\mathrm{out}}\end{aligned} \tag{8}$$

The velocity, the pressure and the density at the inlet of the channel are obtained by the stagnation treatment given by Karki [16]. The stagnation pressure can be expressed in terms of the inlet pressure, velocity and specific internal energy as follows:

$$p_{\mathrm{stg}}=p_{\mathrm{in}}\left[1+\frac{1}{2}\frac{u_{\mathrm{in}}^2}{\gamma i_{\mathrm{in}}}\right]^{\gamma/\gamma-1} \tag{9}$$

Also, from the ideal gas law, the relationship for pressure and density between stagnation and inlet point can be expressed as

$$\frac{p_{\mathrm{stg}}}{\rho_{\mathrm{stg}}^{\gamma}}=\frac{p_{\mathrm{in}}}{\rho_{\mathrm{in}}^{\gamma}} \tag{10}$$

The static pressure at the inlet can be obtained from a linear extrapolation from the interior of the computational domain. By substituting the extrapolated pressure and the stagnation pressure into Eq. (10), the inlet density is obtained. Upon, using the equation of state, the specific internal energy at the inlet can be found. Finally, the inlet velocity can be determined by substituting these values into Eq. (9). The procedure is repeated until convergence is achieved.

The computations were performed with dimensional values. However, the dimensionless form of the governing equations will be introduced to investigate the dimensionless parameters that govern the flow and the friction factor. The following dimensionless variables are used.

$$\begin{aligned}&X=x/D_{\mathrm{h}},\quad Y=y/D_{\mathrm{h}},\quad U=u/\bar{u}_{\mathrm{ref}},\quad V=v/\bar{u}_{\mathrm{ref}},\\&\rho^*=\rho/\bar{\rho}_{\mathrm{ref}},\quad P=(p-\bar{p}_{\mathrm{ref}})/(\bar{\rho}_{\mathrm{ref}}\bar{u}_{\mathrm{ref}}^2),\quad I=i/\bar{i}_{\mathrm{ref}},\\&Re=\frac{\bar{\rho}_{\mathrm{ref}}\bar{u}_{\mathrm{ref}}D_{\mathrm{h}}}{\mu},\quad Ma=\frac{\bar{u}_{\mathrm{ref}}}{\sqrt{\gamma(\gamma-1)\bar{i}_{\mathrm{ref}}}}\end{aligned} \tag{11}$$

where D_{h} is hydraulic diameter. The bar quantities below refer to the average values at the reference cross-section.

$$\begin{aligned}&\bar{u}_{\mathrm{ref}}=\frac{1}{A}\int u_{\mathrm{ref}}\,\mathrm{d}A,\quad \bar{\rho}_{\mathrm{ref}}=\int \rho_{\mathrm{ref}}u_{\mathrm{ref}}\,\mathrm{d}A\Big/\int u_{\mathrm{ref}}\,\mathrm{d}A,\\&\bar{p}_{\mathrm{ref}}=\frac{1}{A}\int p_{\mathrm{ref}}\,\mathrm{d}A,\quad \bar{i}_{\mathrm{ref}}=\frac{1}{\gamma-1}\frac{\bar{p}_{\mathrm{ref}}}{\bar{\rho}_{\mathrm{ref}}}\end{aligned} \tag{12}$$

Using the above dimensionless variables, the governing equations can be expressed as

$$\frac{\partial \rho^* U}{\partial X}+\frac{\partial \rho^* V}{\partial Y}=0 \tag{13}$$

$$\frac{\partial \rho^* UU}{\partial X}+\frac{\partial \rho^* UV}{\partial Y}=-\frac{\partial P}{\partial X}+\frac{1}{Re}\left(\frac{\partial^2 U}{\partial X^2}+\frac{\partial^2 U}{\partial Y^2}\right)+\frac{1}{3Re}\frac{\partial}{\partial X}\left(\frac{\partial U}{\partial X}+\frac{\partial V}{\partial Y}\right) \tag{14}$$

$$\frac{\partial \rho^* UV}{\partial X}+\frac{\partial \rho^* VV}{\partial Y}=-\frac{\partial P}{\partial Y}+\frac{1}{Re}\left(\frac{\partial^2 V}{\partial X^2}+\frac{\partial^2 V}{\partial Y^2}\right)+\frac{1}{3Re}\frac{\partial}{\partial Y}\left(\frac{\partial U}{\partial X}+\frac{\partial V}{\partial Y}\right) \tag{15}$$

$$\frac{\partial \rho^* UI}{\partial X}+\frac{\partial \rho^* VI}{\partial Y}=-(\gamma-1)(\gamma Ma^2 P+1)\left(\frac{\partial U}{\partial X}+\frac{\partial V}{\partial Y}\right)+\gamma(\gamma-1)\frac{Ma^2}{Re}\Phi \tag{16}$$

where Φ is the dissipation function given by

$$\Phi=2\left[\left(\frac{\partial U}{\partial X}\right)^2+\left(\frac{\partial V}{\partial Y}\right)^2\right]-\frac{2}{3}\left(\frac{\partial U}{\partial X}+\frac{\partial V}{\partial Y}\right)^2+\left(\frac{\partial U}{\partial Y}+\frac{\partial V}{\partial X}\right)^2 \tag{17}$$

Also, for the assumption of an ideal gas, the equation of the state is expressed by

$$\rho^*=\frac{1}{I}(\gamma Ma^2 P+1) \tag{18}$$

The friction factors based on the Darcy's and Fanning definitions will be introduced. The Darcy friction factor at the reference cross-section is defined for both the 'no heat conduction' and the isothermal flow conditions as

$$f_{\mathrm{d}}=\frac{-2D_{\mathrm{h}}}{\bar{\rho}_{\mathrm{ref}}\bar{u}^2_{\mathrm{ref}}}\left(\frac{\mathrm{d}\bar{p}}{\mathrm{d}x}\right)_{\mathrm{ref}}=-2\left(\frac{\mathrm{d}\overline{P}}{\mathrm{d}X}\right)_{\mathrm{ref}} \tag{19}$$

This definition of the friction factor includes both the viscous friction loss and the flow acceleration loss.

The following equation is used to evaluate the modified Fanning friction factor (four times of Fanning friction factor) for the no heat conduction flow.

$$\begin{aligned} f_{\mathrm{f}}&=\frac{4\tau_{\mathrm{w}}}{(1/2)\bar{\rho}_{\mathrm{ref}}\bar{u}^2_{\mathrm{ref}}}\\ &=\frac{2D_{\mathrm{h}}}{\bar{p}_{\mathrm{ref}}}\left(\frac{\mathrm{d}\bar{p}}{\mathrm{d}x}\right)_{\mathrm{ref}}-\frac{2D_{\mathrm{h}}}{\bar{\rho}_{\mathrm{ref}}\bar{u}^2_{\mathrm{ref}}}\left(\frac{\mathrm{d}\bar{p}}{\mathrm{d}x}\right)_{\mathrm{ref}}-\frac{2D_{\mathrm{h}}}{T}\left(\frac{\mathrm{d}\overline{T}}{\mathrm{d}x}\right)_{\mathrm{ref}}\\ &=2\left\{\gamma Ma^2\left(\frac{\mathrm{d}\overline{P}}{\mathrm{d}X}\right)_{\mathrm{ref}}-\left(\frac{\mathrm{d}\overline{P}}{\mathrm{d}X}\right)_{\mathrm{ref}}+\frac{2(\gamma-1)Ma}{(\gamma-1)Ma^2+2}\left(\frac{\mathrm{d}Ma}{\mathrm{d}X}\right)_{\mathrm{ref}}\right\} \end{aligned} \tag{20}$$

Eq. (20) is derived using correlations for a one-dimensional compressible flow in an adiabatic channel with a constant cross-section that is called as Fanno flow. Also, the following equation is used to evaluate the modified Fanning friction factor for the isothermal flow.

$$\begin{aligned} f_{\mathrm{f}}&=\frac{4\tau_{\mathrm{w}}}{1/2\bar{\rho}_{\mathrm{ref}}\bar{u}^2_{\mathrm{ref}}}\\ &=\frac{2D_{\mathrm{h}}}{\bar{p}_{\mathrm{ref}}}\left(\frac{\mathrm{d}\bar{p}}{\mathrm{d}x}\right)_{\mathrm{ref}}-\frac{2D_{\mathrm{h}}}{\bar{\rho}_{\mathrm{ref}}\bar{u}^2_{\mathrm{ref}}}\left(\frac{\mathrm{d}\bar{p}}{\mathrm{d}x}\right)_{\mathrm{ref}}\\ &=2\left\{\gamma Ma^2\left(\frac{\mathrm{d}\overline{P}}{\mathrm{d}X}\right)_{\mathrm{ref}}-\left(\frac{\mathrm{d}\overline{P}}{\mathrm{d}X}\right)_{\mathrm{ref}}\right\} \end{aligned} \tag{21}$$

Eq. (21) is derived using the correlations for a one-dimensional compressible isothermal flow (e.g., [17]). The definition of the Fanning friction factor includes only the viscous wall friction loss and the first term on the right-hand side of Eqs. (20) and (21) represents the acceleration loss. It is well known that the friction factor for incompressible flow in the fully developed region is function of *Re* number. However, from the examination of Eqs. (13)–(21), it can be seen that friction factor for the compressible flow is function of *Re* and *Ma* numbers at the reference cross-section. It is also true that the friction factor is a function of stagnation pressure, stagnation temperature and the location of x.

2.2. Numerical solutions

The numerical methodology is based on arbitrary-Lagrangian–Eulerian (ALE) method proposed by Amsden et al. [18]. The detailed description of the ALE method is documented in [18] and will not be given here. The computational domain is divided into quadrilateral cells. The velocity components are defined at the vertices of the cell and other variables such as pressures, specific internal energy and density are assigned at the cell centers. The number of cells in the x-direction was 100 or 200 depending on the aspect ratio of the channel. The cell size gradually increased in the x-direction along the channel. The number of cells in y-direction was fixed at 20 for all the computations. The ALE method is a time marching method. The value of 10^{-4} was used for the convergence criterion of Newton–Raphson iteration.

Supplementary runs were performed with coarse cells (50×10) and fine cells (200×40) to investigate the cell size effect on Ma, $f_{\mathrm{f}}\cdot Re$ and $f_{\mathrm{d}}\cdot Re$. For the height and the length of the channel of $h=20$ μm and $\ell=1000$ μm, the values of Ma, $f_{\mathrm{f}}\cdot Re$ and $f_{\mathrm{d}}\cdot Re$ at $x=500$ μm were examined. The computations were performed for air flow under the stagnation condition of $p_{\mathrm{stg}}=10^5$ Pa, and $T_{\mathrm{stg}}=300$ K and with $p_{\mathrm{out}}=5\times10^4$ Pa. The results are tabulated in Table 1. The maximum change in the values between the medium cells (100×20) and the fine cells were 1.28%. Therefore, all the computations were performed for (100×20) or (200×20) cells.

Table 1
Effect of cell size on Ma, $f_{\mathrm{f}}\cdot Re$ and $f_{\mathrm{d}}\cdot Re$

	Ma	$f_{\mathrm{f}}\cdot Re$	$f_{\mathrm{d}}\cdot Re$
Coarse cells (50×10)	0.215	99.9	106.9
Medium cells (100×20)	0.210	100.5	107.1
Fine cells (200×40)	0.209	99.3	105.7
Change between coarse and medium cells	2.34%	−0.53%	−0.19%
Change between fine and medium cells	−0.48%	−1.20%	−1.28%

3. Results and discussions

The computations were performed for four microchannels with air of $R = 287$ J/(kg K), $\gamma = 1.4$ and $\mu = 1.862 \times 10^{-5}$ Pa s. The channel height and length are tabulated in Table 2. The stagnation condition was fixed at $p_{stg} = 10^5$ Pa and $T_{stg} = 300$ K for all channels. The static outlet pressure, p_{out} was varied, namely, several computations were performed for each channel. The range of the outlet pressure, p_{out} is also listed in Table 2. Supplementary runs were performed for 10, 20 and 50 μm channels under two different stagnation conditions of $p_{stg} = 2 \times 10^5$ Pa and $T_{stg} = 300$ K and $p_{stg} = 10^5$ Pa and $T_{stg} = 150$ K to investigate the effect of the stagnation values.

3.1. Pressure and temperature distributions and velocity vector

The contour plots of the pressure and temperature for the flow in the channel of $h = 20$ μm and $\ell = 1000$ μm are presented in Fig. 2(a) and (b), respectively, and the velocity vector is presented in Fig. 2(c). The reference arrow in the figure represents a velocity of 100 m/s. The results are for the 'no heat conduction' flow condition and for the outlet pressure, $p_{out} = 5 \times 10^4$ Pa. As seen in Fig. 2(a), the pressure at any cross-section of the channel is almost uniform, and it decreases along the channel. The pressure gradient along the channel increases gradually. Fig. 2(c) shows the gas flow with a uniform velocity at the inlet. Because of the viscosity, the velocity on the wall is zero and the velocity profile is nearly parabolic. However, the flow in the channel is accelerated and the average velocity increases. This is due to the volume expansion of the gas caused by the pressure drop.

Table 2
Channel dimensions and outlet pressure

Channel	h (μm)	ℓ (mm)	p_{out} (kPa)
#1	10	0.5	3×10^4–9×10^4
#2	20	1	3×10^4–9×10^4
#3	50	5	3×10^4–9×10^4
#4	100	10	9×10^4–9.5×10^4

Fig. 2(b) represents the temperature contours in the channel. The temperature in the core region of the channel decreases as a result of acceleration. On the other hand, the temperature rise can be seen near the walls due to viscous heat dissipation. Since the velocity profile is almost parabolic as shown in Fig. 2(c), the viscous heat dissipation term ϕ can be approximated as

$$\phi \approx \mu\left(\frac{\partial u}{\partial y}\right)^2 = \mu\left(12\bar{u}\frac{y}{h^2}\right)^2 \tag{22}$$

The cell center adjacent to the wall is at $y = (19/20)(h/2)$ because the channel is divided to 20 equal cells in the y-direction. The order of magnitude of ϕ near the exit

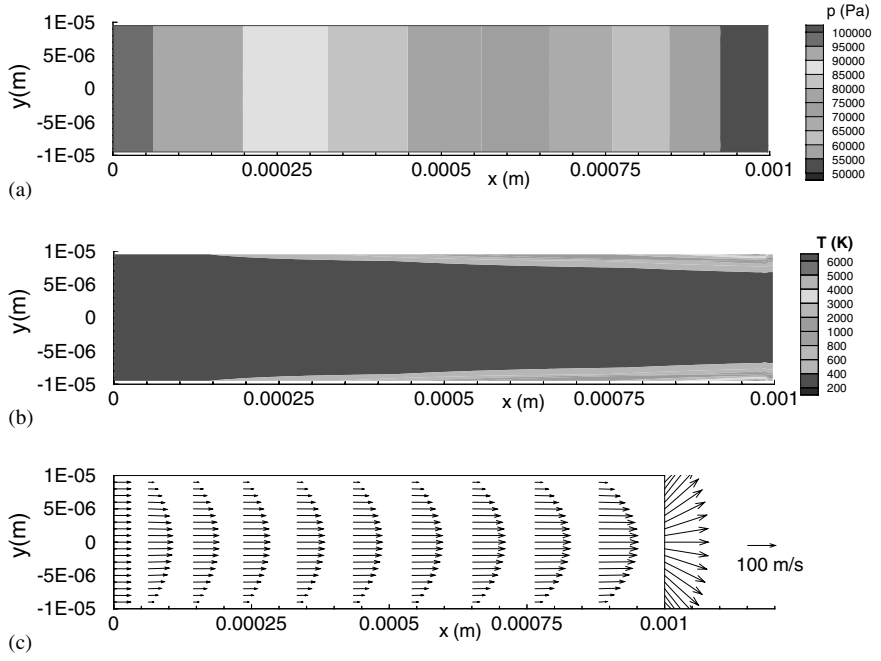

Fig. 2. Contour plots of (a) pressure, (b) temperature and (c) velocity vector (no heat conduction flow: $h = 20$ μm, $\ell = 1000$ μm and $p_{out} = 5 \times 10^4$ Pa).

becomes 1.5×10^{10} W/m^3 for the case of $h = 20$ μm and $\bar{u} = 100$ m/s.

The time to pass through the unit length of the channel can be expressed as

$$t = \frac{1}{u} \tag{23}$$

The velocity at the cell center adjacent to the wall is about 14.6 m/s. Therefore, the heat generation of the cell becomes of order of

$$q = \phi \cdot t = 10^9 \text{ J/m}^3 \tag{24}$$

Using the relationship, $q = \rho c_p \Delta T$, the temperature rise, ΔT, for the fluid passing through the unit length of the channel, is about 3×10^7 K/m. Therefore, the temperature rise per 1 mm becomes 3×10^4 K/mm. Since the average velocity at the inlet is about 50 m/s, the temperature rise might be lower than 3×10^4 K/mm and temperatures of order of magnitude of 6000 K in Fig. 2(b) is reasonable.

3.2. Velocity profile

The velocity profile at $x = 800$ μm is plotted in Fig. 3 for the channel in Fig. 2. The solid line in the figure is a parabola whose value at $y = 0$ coincide with the velocity at $y = 0$. Namely, the solid line represents the velocity profile for the fully developed flow of the incompressible fluid. As seen from the figure, the velocity profile of the compressible flow is not an exact parabola. The velocity of the compressible flow near the wall is faster than the incompressible flow condition and slightly higher friction factor is predicted.

3.3. $f_f \cdot Re$ and $f_d \cdot Re$

The product of the friction factor and Re, $f_\mathrm{f} \cdot Re$ and $f_\mathrm{d} \cdot Re$, and the Mach number are plotted in Fig. 4 as the function of x. Fig. 4(a) is the result for the 'no heat conduction' flow condition in the channel of $h = 20$ μm and $\ell = 1000$ μm and $p_\mathrm{out} = 5 \times 10^4$ Pa with Reynolds number of 139.7. Fig. 4(b) is the result for the isothermal flow condition for the same channel whose Reynolds number is 141.6. As seen from the figures, the channel can be divided into three regions. The region from inlet to $x = 100$ μm can be considered as the entrance region where the friction factor decreases sharply for both cases. The region from $x = 100$ to 900 μm can be considered as the quasi-fully developed region. The last region, from $x = 900$ μm to the exit, can be considered as the exit region where the numerical instability can be seen. The Reynolds number is constant along the channel, as seen from the figure and the Ma number increases along the channel due to the acceleration of the flow. As can be seen $f_\mathrm{f} \cdot Re$ and $f_\mathrm{d} \cdot Re$ increase along the channel and the value of $f_\mathrm{d} \cdot Re$ is slightly higher than that of $f_\mathrm{f} \cdot Re$, because $f_\mathrm{d} \cdot Re$ includes the acceleration loss effect.

The values of $f_\mathrm{f} \cdot Re$ at $x = 0.4\ell$, 0.6ℓ and 0.8ℓ for each channel are presented in form of a contour plot in Fig. 5 and the values of $f_\mathrm{d} \cdot Re$ are plotted in Fig. 6. In both figures, the results for 'no heat conduction' and

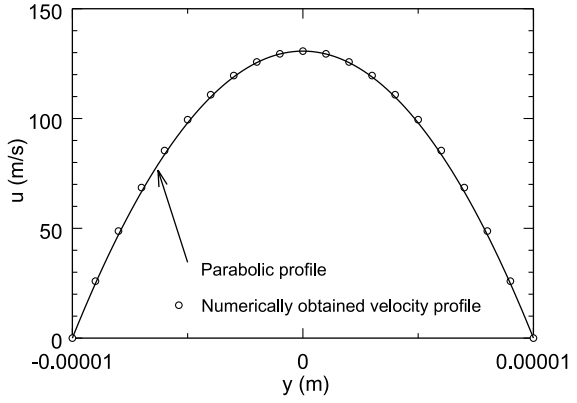

Fig. 3. Velocity profile (u) at $x = 800$ μm (no heat conduction flow).

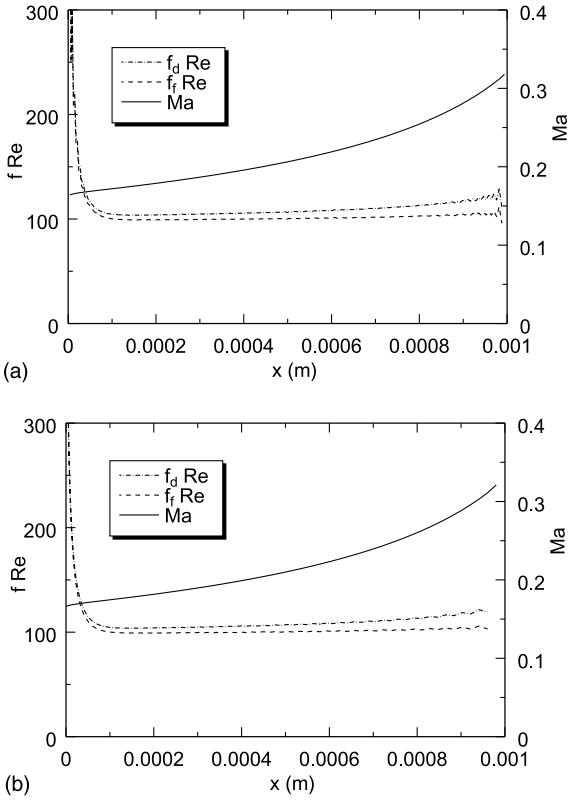

Fig. 4. $f \cdot Re$ and Ma number as a function of axial length (a) no heat conduction flow and (b) isothermal flow.

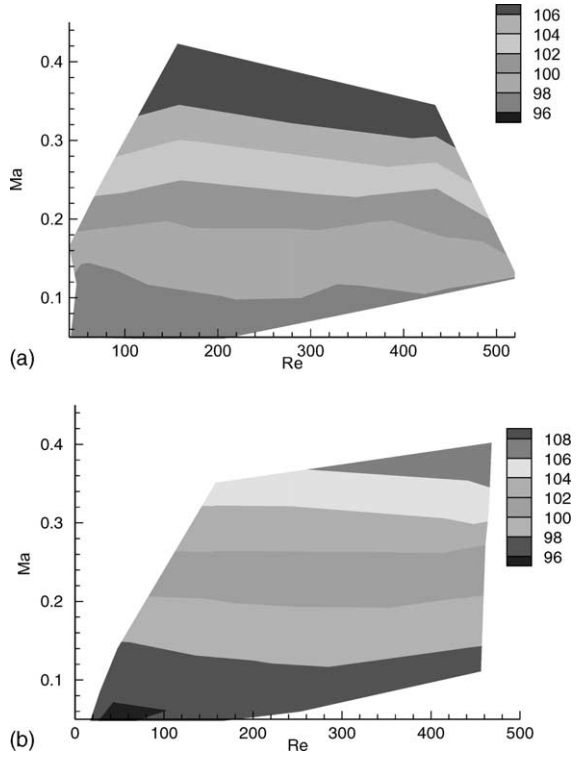

Fig. 5. Contour plot of $f_f \cdot Re$ (a) no heat conduction flow and (b) isothermal flow.

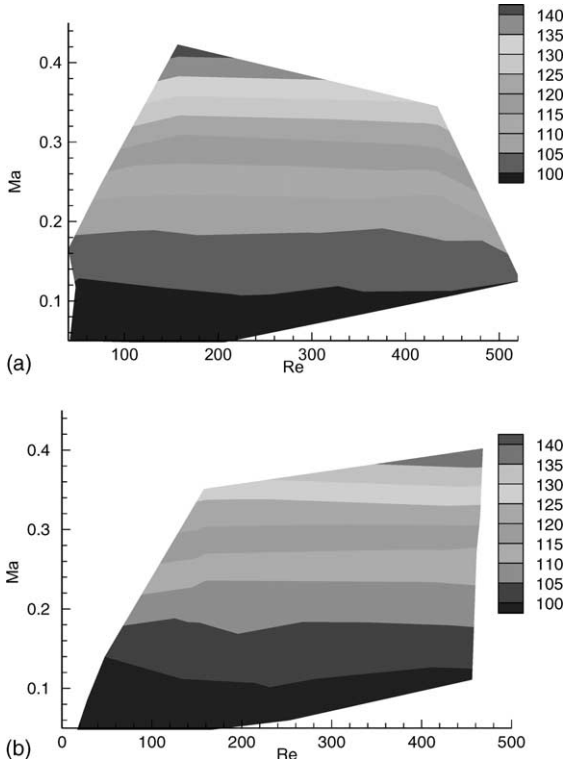

Fig. 6. Contour plot of $f_d \cdot Re$ (a) no heat conduction flow and (b) isothermal flow.

isothermal flow conditions are presented in (a) and (b), respectively. It can be seen that $f_f \cdot Re$ and $f_d \cdot Re$ are mainly function of the Ma number and the effect of Re number is small. The difference between the no heat conduction, and isothermal flow conditions is quite small. The value of $f_f \cdot Re$ in the range of $Ma < 0.05$ is nearly 96 for both cases. The value of $f_f \cdot Re$ at $Ma \approx 0.4$ approaches 106. The value of $f_d \cdot Re$ at $Ma \approx 0.4$ approaches 140.

3.4. Correlation for $f \cdot Re$ and Ma number

The values of $f_f \cdot Re$ and $f_d \cdot Re$ are plotted as a function of Ma number in Fig. 7(a) and (b), respectively. The results for the no heat conduction and isothermal flow conditions are plotted in the same figure. The solid line in the figure represents the correlation for the $f \cdot Re$ and Ma number that is obtained by a polygonal curve fit as:

$$f_f \cdot Re = 96 + 8.17 \times Ma + 59.57 \times Ma^2 \quad (25)$$

$$f_d \cdot Re = 96 - 4.55 \times Ma + 274.8 \times Ma^2 \quad (26)$$

The dashed lines in Fig. 7(a) represent the range of $\pm 2\%$ of Eq. (25). As seen in the figure, most of $f_f \cdot Re$ are within the range of $\pm 2\%$. This is also true for $f_d \cdot Re$.

3.5. Effect of p_{stg} and T_{stg}

The values of $f_f \cdot Re$ and $f_d \cdot Re$ for the isothermal flow condition are plotted as a function of Ma number in Fig. 8(a) and (b), respectively. The computations were performed for two sets of the stagnation values, $p_{stg} = 2 \times 10^5$ Pa and $T_{stg} = 300$ K and $p_{stg} = 1 \times 10^5$ Pa and $T_{stg} = 150$ K. The solid line in the figure represents the correlation between $f \cdot Re$ and Ma number for $p_{stg} = 10^5$ Pa and $T_{stg} = 300$ K and the dashed lines represent the $\pm 2\%$ deviation from the correlations. As seen in the figure, almost all values of $f \cdot Re$ are in the range of $\pm 2\%$. It can be concluded that the effect of the stagnation values on $f \cdot Re$ is small. The results for the no heat conduction flow condition are not shown in the figure but are similar. Namely, all values of $f \cdot Re$ for the no heat conduction flow condition coincide with the correlation for $p_{stg} = 10^5$ Pa and $T_{stg} = 300$ K to within $\pm 2\%$.

3.6. Comparisons with experimental data

Turner et al. [15] measured local pressure of nitrogen, helium and air flows along micro-channels with a rectangular cross-section. The inlet pressure was varied

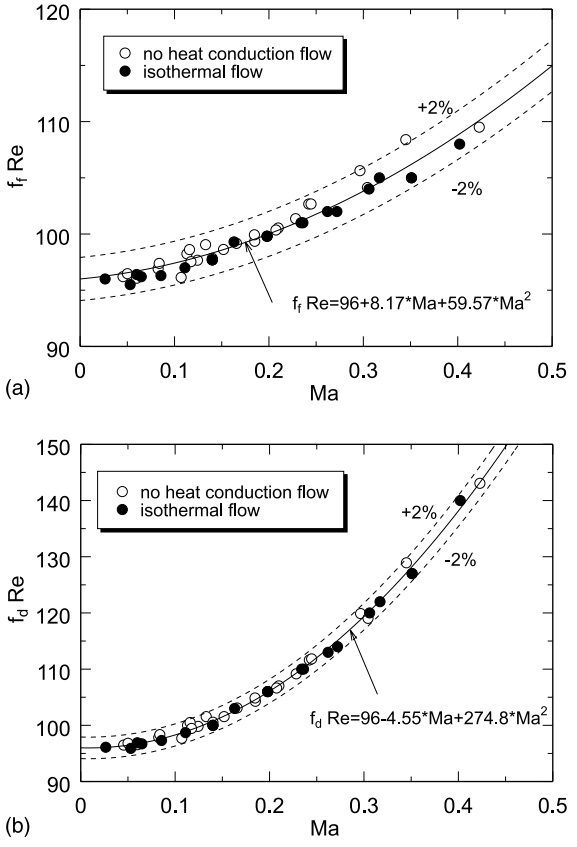

Fig. 7. $f_f \cdot Re$ and $f_d \cdot Re$ as a function of Ma number (a) $f_f \cdot Re$ and (b) $f_d \cdot Re$.

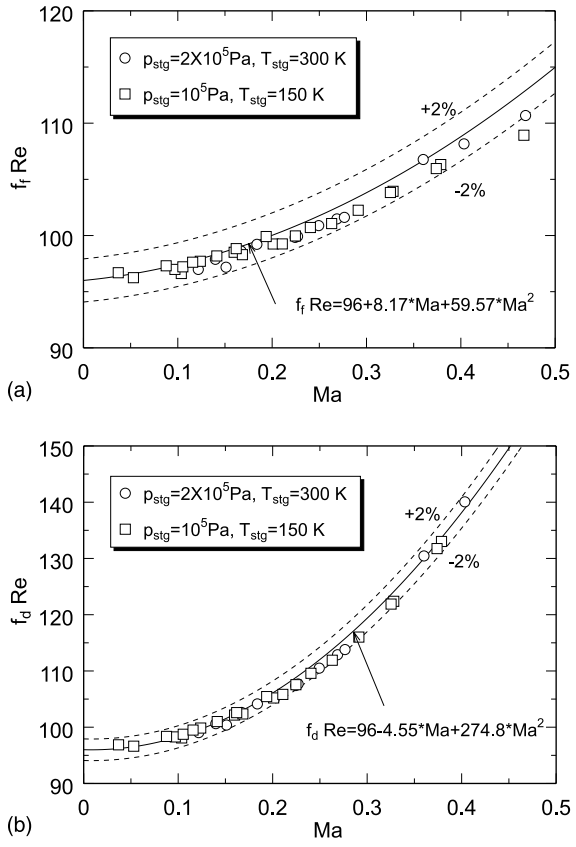

Fig. 8. Effect of p_{stg} and T_{stg} on $f \cdot Re$ of isothermal flow (a) $f_f \cdot Re$ and (b) $f_d \cdot Re$.

between 135 and 700 kPa with the outlet pressure maintained at atmospheric condition. The micro-channel were etched into silicon wafers and capped with smooth glass. The channel length was about 27 mm and the hydraulic diameter ranges from 4 to 100 μm. Five pressure taps were equipped along the channel with equal spacing of 5 mm and additional two pressure taps were located at the inlet and outlet ports. The details of the experiment were well documented in the previous papers [14,15].

The average friction factor between the first and fifth pressure taps in the channel were obtained and the product of the average friction factor and Reynolds number, $f_f \cdot Re$, were reported in the literature. The semi-local friction factor based on the pressure differences between pressure taps was not reported in the previous papers. Therefore in this paper, the semi-local friction factors were obtained from the pressure data, for nitrogen flow through a channel with height, width and length of 50 μm, 994 μm and 26.87 mm, respectively. The relative surface roughness, ε/H, of the channel was 0.001. The inlet port pressure was set between 140 and 320 kPa for nitrogen and the outlet pressure maintained at atmospheric condition.

A computation was performed for same flow conditions and channel dimensions as the experimental data. Namely, the flow was assumed to be an isothermal flow and the computational parameters were $R = 296.7$ J/(kg K), $\gamma = 1.399$, $\mu = 1.777 \times 10^{-5}$ Pa s, $p_{stg} = 1.47 \times 10^5$ Pa, $T_{stg} = 295.9$ K and $p_{out} = 1.009 \times 10^5$ Pa. The pressure distribution along the channel is presented in Fig. 9 with the experimental data. The numerical result coincides well with experimental data. The semi-local friction factors between third and fourth pressure taps and between fourth and fifth pressure taps were evaluated from the experimental data using Eq. (21). The results are presented in form of $f_f \cdot Re/f_f \cdot Re_{incomp}$ in Fig. 10. The product of the friction factor and Reynolds number for the incompressible flow, $f_f \cdot Re_{incomp}$ for the same channel geometry is 89.85 (e.g., [19]). The correlation given by Eq. (25) is also plotted in this figure. A small discrepancy between the correlation and the ex-

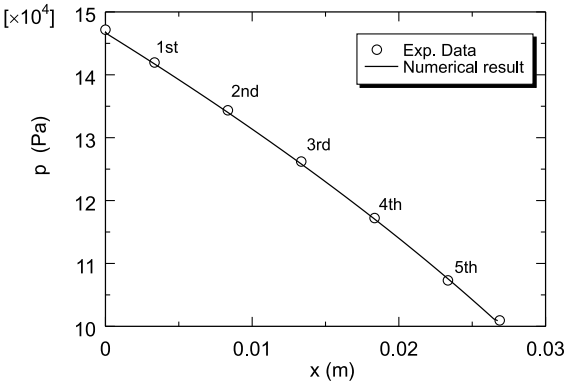

Fig. 9. Pressure distribution along channel.

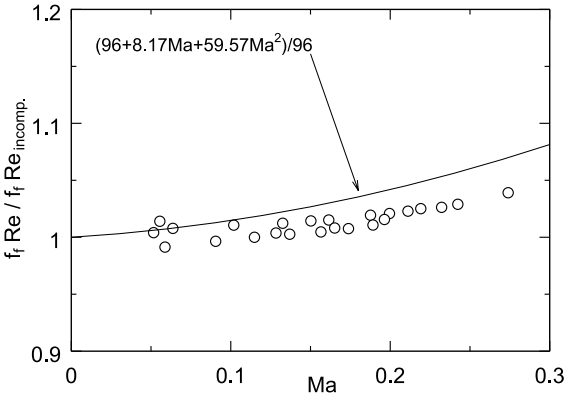

Fig. 10. Comparison of $f_f \cdot Re/f_f \cdot Re_{incomp}$ with experimental data.

perimental data can be seen. However, the correlation and the experimental data have similar trends, namely, $f_f \cdot Re$ increases with increasing local Ma number.

4. Concluding remarks

Two-dimensional compressible momentum and energy equations are solved for a parallel-plate microchannel. The computations were performed for no heat conduction and isothermal flow conditions. The following conclusions are reached.

1. Both $f_f \cdot Re$ and $f_d \cdot Re$ are function of the Mach number and they differ from the incompressible value of 96 for parallel-plate ducts. The following correlations are obtained for $P_{stg} = 10^5$ Pa and $T_{stg} = 300$ K in the range of $Re < 500$ and $Ma < 0.4$.

$$f_f \cdot Re = 96 + 8.17 \times Ma + 59.57 \times Ma^2$$

$$f_d \cdot Re = 96 - 4.55 \times Ma + 274.8 \times Ma^2$$

2. The effect of stagnation pressure and temperature on $f \cdot Re$ is small. The values of $f_f \cdot Re$ and $f_d \cdot Re$ for both cases of $p_{stg} = 2 \times 10^5$ Pa and $T_{stg} = 300$ K and $p_{stg} = 10^5$ Pa and $T_{stg} = 150$ K coincide with the values under $p_{stg} = 10^5$ Pa and $T_{stg} = 300$ K to within ±2%.

References

[1] D.B. Tuckerman, R.F.W. Pease, High-performance heat sinking for VLSI, IEEE Electron Dev. Lett. EDL-2 (5) (1981) 126–129.
[2] P. Wu, W.H. Little, Measurement of friction factors for the flow of gases in very fine channels used for micro miniature Joule–Thompson refrigerators, Cryogenics (1983) 273–277.
[3] J. Pfahler, J. Harley, H. Bau, J.N. Zemel, Gas and liquid flow in small channels, in: Proceedings of ASME Winter Annual Meeting, Micro Mech. Sensors Actuat. Syst. DSC 32 (1991) 49–60.
[4] S.B. Choi, R.F. Barron, R.O. Warrington, Fluid flow and heat transfer in micro tubes, in: Proceedings of ASME Winter Annual Meeting, Micro Mech. Sensors Actuat. Syst. DSC 32 (1991) 123–134.
[5] E.B. Arkilic, M.A. Schmidt, K.S. Breuer, Gaseous flow in micro channel, in: ASME Symposium on Micro Machining and Fluid Mechanics, 1994, pp. 1–10.
[6] A. Bebkok, G.E. Karniadakis, Simulation of heat and momentum transfer in complex micro geometries, J. Thermophys. Heat Transfer 8 (4) (1994) 647–655.
[7] R.K. Prud'homme et al., Laminar compressible flow in a tube, Appl. Sci. Res. 43 (1986) 67–74.
[8] H.R. Berg, C.A. Seldam, P.S. Gulik, Compressible laminar flow in a capillary, J. Fluid Mech. 246 (1983) 1–20.
[9] R. Sayegh et al., Direct simulation Monte Carlo of gaseous flow in micro-channel, in: 33rd National Heat Transfer Conference, HTD99-256, 1999, pp. 1–10.
[10] H. Sun, M. Faghri, Effect of rarefaction and compressibility of gaseous flow in micro channel using DSMC, Numer. Heat Transfer, Part A 38 (2000) 153–158.
[11] Z.Y. Guo, X.B. Wu, Compressibility effect on the gas flow and heat transfer in a micro tube, Int. J. Heat Mass Transfer 40 (13) (1997) 3251–3254.
[12] T. Araki et al., An experimental investigation of gaseous flow characteristics in microtubes, in: Proceedings of Kyoto University–Tsinghua University Joint Conference on Energy & Environment, 1999, pp. 7–12.
[13] T. Araki et al., An experimental investigation of gaseous flow characteristics in microchannels, in: Proceedings of International Conference on Heat Transfer and Transport Phenomena in microscale, 2000, pp. 155–161.
[14] S.E. Turner, H. Sun, M. Faghri, O.J. Gregory, Effect of surface roughness on gaseous flow through micro channels, 2000 IMECE, HTD., vol. 366 (2) (2000) 291–298.
[15] S.E. Turner, H. Sun, M. Faghri, O.J. Gregory, Compressible gas flow through smooth and rough microchannels, 2001 IMECE, HTD-24145, 2001, pp. 1–4.

[16] K.C. Karki, A calculation procedure for viscous flows at all speeds in complex geometries, PhD Thesis, University of Minnesota, 1986.
[17] S.F. Choquette et al., Compressible fluid flow in micron sized channels, ASME HTD, vol. 327 (1996) 25–32.
[18] A.A. Amsden et al., SALE a simplified ALE computer program for fluid flow at all speeds, Los Alamos Scientific Lab. Report, LA-8095, 1980.
[19] R.K. Shah, A.L. London, Laminar flow forced convection in ducts, in: Advances in Heat Transfer Supplement 1, Academic Press, New York, 1978.